Toward Efficient Water/Oil Separation Material: Effect of Copolymer Composition on pH-Responsive Wettability and Separation Performance

Yin-Ning Zhou, Jin-Jin Li, and Zheng-Hong Luo
Dept. of Chemical Engineering, School of Chemistry and Chemical Engineering, Shanghai Jiao Tong University, Shanghai 200240, P.R. China

DOI 10.1002/aic.15145
Published online January 5, 2016 in Wiley Online Library (wileyonlinelibrary.com)

Interest in functional soft matter with stimuli-responsive wettability has increasingly intensified in recent years. From the chemical product engineering viewpoint, this study aims to fabricate reversible pH-responsive polymeric surfaces with controllable wettability using [poly(2,2,3,4,4,4-hexafluorobutyl methacrylate)-block- poly(acrylic acid) (PHFBMA-b-PAA)] block copolymers. To attain this aim, three block copolymers with different PAA segment lengths were synthesized for the first time through Cu(0)-mediated reversible-deactivation radical polymerization and hydrolysis reaction. pH-induced controllable wettability was achieved by spin-coating the resulting block copolymers onto silicon wafers. Results showed that the pH-responsive wetting behavior was introduced by incorporating the PAA block, and that the responsiveness of as-fabricated surfaces was greatly influenced by PAA content. All three evolutions of water contact angle with pH shared a similar inflection point at pH 5.25. Furthermore, on the basis of the wetting properties and mechanism understanding, the application of copolymer coated meshes in layered water/oil separation was exploited. Given their superhydrophilicity and underwater superoleophobicity, $PHFBMA_{70}$-b-PAA_{148} and $PHFBMA_{70}$-b-PAA_{211} coated stainless steel meshes (SSMs) can efficiently separate water from different mixtures of organic solvent and water with high flux. However, considering long-term use, the $PHFBMA_{70}$-b-PAA_{148} coated SSM with good stability may be the best copolymer for water/oil separation. Therefore, a coordination of structure, composition, and functionality was necessary to enable practical applications of the functional materials. *AIChE J*, 62: 1758–1771, 2016
Keywords: soft matter, fluorinated polymer, Cu(0)-mediated reversible-deactivation radical polymerization, pH-responsive hydrophilic surface, oil/water separation

Introduction

Multifunctional or stimuli-responsive polymeric materials, which belong to soft matters, have become a research hotspot because of their wide-ranging applications from the chemical product viewpoint.[1–3] One such smart material is the stimuli-responsive polymeric surface with tunable wettability under different external conditions,[4] such as pH,[5–8] electric potential,[9,10] light,[11–14] temperature,[15–18] and gas.[19] This feature enables the material to have applications in many areas, including controlled release platform,[20] ion pump,[21] and water/oil separation.[22–24]

pH-responsive method is an attractive method to trigger the change of wettability due to its rapid response process.[4] For example, Wu and coworkers.[6] fabricated a smart surface with reversible pH-responsive wettability using polybase- and polyacid-based polymers. Hozumi and coworkers[7,8] highlighted the pH-responsive superoleophobicity of poly[2-(dimethylamino)ethyl methacrylate] brush surfaces, giving excellent oil drop mobility and low adhesion underwater. Wang and coworkers[22] and Lu and coworkers[23] reported advanced materials with switchable wettability by grafting block copolymer containing pH-responsive poly(2-vinylpyridine) segments on nonwoven textile and graphene foam respectively for water/oil separations. However, the surface grafting method is complex, and thus limits its practical application. Compared with the polymer grafting, functional polymer coating that can be used directly would be more attractive in industrial fields because of its simple implementation process.[12–15] More recently, Yuan and Luo et al. fabricated two types of smart fiber membranes by depositing pH-responsive copolymer fibers on a stainless steel mesh (SSM) through electrospinning for controllable oily water separation.[19,24]

Poly(acrylic acid) (PAA) is a typical pH-sensitive hydrophilic polymer with pKa = 4.7.[25] Previous study showed that PAA chain conformation can change from the collapsed structure at pH < pKa to the stretched state at pH > pKa through protonation and deprotonation of carboxyl groups.[25,26] With the aid of pH-responsive feature of PAA, PAA containing

Additional Supporting Information may be found in the online version of this article.

Correspondence concerning this article should be addressed to Z.-H. Luo at luozh@sjtu.edu.cn.

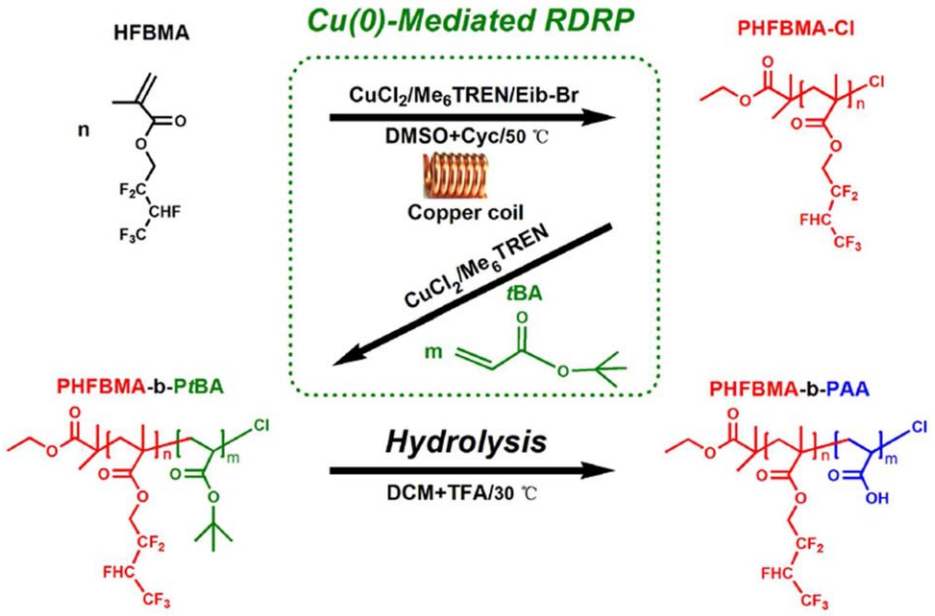

Scheme 1. Synthesis route of PHFBMA-*b*-PAA block copolymer.

[Color figure can be viewed in the online issue, which is available at wileyonlinelibrary.com.]

copolymers are able to be used for responsive colloidal microgel,[27,28] self-assembly in aqueous solution on the pH of surrounding circumstance.[29,30] and especially the surfaces with switchable wettability.[31,32] Further studies including dissociation, switching and swelling behaviors, have been performed to reveal the pH-responsive mechanism of pure PAA grafting surface.[26,33–37] However, the surfaces coated with hydrophilic homopolymers are unstable in the aqueous medium. To extend the application range of hydrophilic PAA coated surface, incorporating a water-insoluble component into polymer chains is needed. Given the unique properties, such as excellent chemical and thermal stability, fluorinated and semifluorinated polymers have received a great deal of interests from both academic and industrial fields.[38,39] Through a careful design, the resulting fluorinated polymers endow surfaces with low-adhesive, antifouling and stimuli-responsive properties.[40–46]

Bearing this in mind, we aim to fabricate reversible pH-responsive polymeric surfaces with controllable wettability based on block copolymers [poly(2,2,3,4,4,4-hexafluorobutyl methacrylate)-block-poly(acrylic acid) (PHFBMA-*b*-PAA)]. In terms of the chemical product engineering perspective, this study covers the following: the design and preparation polymer, product characterization, property analysis, and application study. Coating materials, PHFBMA-*b*-PAA with different PAA segment lengths, were first synthesized. Cu(0)-mediated reversible-deactivation radical polymerization [Cu(0)-mediated RDRP] was chosen as the method for polymerization due to some distinct advantages over other RDRP techniques, such as simple experimental setup, moderate conditions, and reusability of the Cu(0) sources.[47–50] The synthesis route is illustrated in Scheme 1. Subsequently, the performances of the polymer surfaces fabricated by the copolymers with different PAA segment lengths were evaluated, including switchable pH-responsive wettability, surface composition, and surface morphology. Finally, based on the wetting properties and mechanism understanding, the application of copolymer coated meshes in water/oil separation was exploited. Also, the best copolymer for efficiently separating water from a water/oil mixture based on the resulting copolymer coated mesh was identified.

Experimental

Materials

2,2,3,4,4,4-Hexafluorobutyl methacrylate (HFBMA, Xeogia Fluorine-Silicon Chemical Co. Ltd., China, 96%) and *t*-butyl acrylate (*t*BA, 99%, Sinopharm Chemical Reagent Co., Ltd [SCRC]) were rinsed with an aqueous NaOH (5 wt %) solution and then with deionized water to remove inhibitor prior to use. Copper (wire, diameter 1.0 mm, 99.9%, Alfa Aesar) was typically activated by methanol/HCl solution first and then rinsed with methanol prior to use. Ethyl 2-bromoisobutyrate (Eib-Br, 98%, Alfa Aesar), hexamethylated tris(2-aminothyl) amine (Me_6TREN, 99%, Alfa Aesar), $CuCl_2$ (99%, Acros), and trifluoroacetic acid (TFA, 99%, SCRC) were used as received. Other reagents with analytical pure were used as received without further purification. The SSM with 350 mesh sizes was cleaned by ethanol- and acetone-rinsing prior to use.

Synthesis of macroinitiator PHFBMA-Cl

The first block was prepared by Cu(0)-mediated RDRP. A magnetic stirrer winded by activated Cu(0) wire (4 cm) and $CuCl_2$ (0.90 mg, 6.7×10^{-3} mmol) were placed in a Schlenk flask, degassed and full filled with nitrogen for three times. The mixed solvent (3.0 mL) consisting of dimethyl sulfoxide (DMSO)/cyclohexanone (cyc) with the volume ratio of 1:1 and monomer HFBMA (5.0 mL, 27 mmol) were bubbled by nitrogen for 30 min, and then were added to the flask. The mixture was deoxygenated by three freeze-pump-thaw cycles. At last, Me_6TREN (17 μL, 6.7×10^{-2} mmol) and initiator (Eib-Br, 39 μL, 0.27 mmol) were sequentially added under nitrogen protection. The reaction mixture was stirred in an oil bath with a thermostat at 50 °C. The reaction was stopped by quenching in liquid nitrogen and exposing to air. The polymer solution was diluted with chloroform and passed through a neutral alumina column to remove the copper complex. The purified product was obtained through repeated dissolution in

chloroform and precipitation in 3M hydrochloric acid (HCl)-methanol solution for three times and dried under vacuum.

Synthesis of PHFBMA-b-PtBA

The block copolymer was prepared through sequential Cu(0) mediated RDRP using macroinitiator PHFBMA-Cl. To a Schlenk flask, PHFBMA-Cl (1.0 g, 5.7×10^{-2} mmol) was first dissolved in deoxygenated DMSO/cyc mixed solvent (5 mL) with the volume ratio of 1:1. After that, a magnetic stirrer winded by activated Cu(0) wire (4 cm) and $CuCl_2$ (0.51 mg, 3.8×10^{-3} mmol) were added into the flask and subjected to three freeze-vacuum-thaw cycles. Finally, Me_6TREN (10 μL, 3.8×10^{-2} mmol) and *t*BA (2.1 mL, 14.5 mmol) were sequentially added under nitrogen protection. The reaction mixture was stirred at 50 °C for a certain time and stopped by quenching in liquid nitrogen and exposing to air. The polymer solution was diluted with chloroform and passed through a neutral alumina column to remove the copper complex. The purified product was obtained through repeated dissolution in chloroform and precipitation in 3M hydrochloric acid (HCl)-methanol solution for three times and dried under vacuum.

Hydrolysis of PHFBMA-b-PtBA

The block copolymer PHFBMA-*b*-P*t*BA was dissolved in dry dichloromethane (DCM) and followed by adding a five-fold molar excess of TFA. The solution was stirred at 30 °C for 24 h. The hydrolyzate (PHFBMA-*b*-PAA) was precipitated from DCM. The purified product was obtained through repeated dissolution in tetrahydrofuran and precipitation in petroleum ether (60–90 °C), and dried under vacuum.

Preparation of copolymer films

Block copolymer coated silicon wafers were prepared by spin-coating a polymer solution (5 wt % in THF) onto clean silicon wafers at 3000 rpm for 30s. The thickness of the spin-coated films measured by atomic force microscope (AFM) is 150 ± 8 nm. The results for different samples are statistically analyzed using three readings from different cross-sections. Block copolymer coated mesh was prepared by solution-casting a polymer solution (5 wt % in THF) onto clean SSM directly. The samples were dried naturally until most of solvent evaporated, and then dried under vacuum at 60 °C for another 24 h.

Instrumentation and characterization

^{1}H NMR was recorded on a Bruker Avance III HD 400, 400 MHz NMR spectrometer. Molecular weights and molecular weight distributions (M_w/M_n) of polymers were measured on a size exclusion chromatography (SEC, Tosoh Corporation) equipped with two HLC-8320 columns (TSK gel Super AWM-H, pore size: 9 μm; 6 × 150 mm, Tosoh Corporation) and a double-path, double-flow a refractive index detector (Bryce) at 30 °C. The thermal analysis of the copolymers was performed using a differential scanning calorimeter (TA Instruments Q2000) under a dry nitrogen atmosphere. The samples were first heated at a rate of 10 °C/min from 0 °C to 200 °C and held at 200 °C for 3 min to eliminate thermal history. All data associated with the glass transition temperature (T_g) measurements were obtained from the second heating scan and taken as the midpoint of heat capacity change. Surface morphology, roughness and thickness of the spin-coated films were acquired on an AFM measurement using a Dimension Icon scanning probe microscope equipped with Nanoscope V controller (Bruker) in the tapping mode at room temperature in air. X-ray photoelectron spectroscopy (XPS) spectra were acquired through a Kratos Axis Ultra DLD spectrometer (Kratos Analytical-A Shimadzu group company) using a monochromatic Al Kα x-ray beams as the excitation source (1486.6 eV). The analyzer uses hybrid magnification mode (both electrostatic and magnetic) and take-off angle is 90°. The morphologies of the films were observed on a JEOL JSM-7500F field emission scanning electron microscope (FE-SEM). All these static contact angles of as-prepared surfaces were measured on a Kruss DSA30 contact angle measurement at room temperature. It should be noted that because of the heterogeneity of all surfaces investigated in this work, all obtained contact angles are apparent contact angles, rather than the Young' equilibrium contact angles.

Results and Discussion

Synthesis and characterization of Polymers

First, macroinitiator PHFBMA-Cl was prepared through Cu(0)-mediated RDRP under optimized experimental conditions.[51] The ^{1}H NMR spectrum (red) shown in Figure 1A indicates that all the peaks are assigned to their corresponding groups without discernable impurity, which guarantees the next step of polymerization. The signals for the methyne protons (-C*H*F-) of hexafluorobutyl methacrylate and the methylene protons (-CH_2-) of ethyl 2-bromoisobutyrate are located at 4.70–5.20 ppm and 4.00–4.20 ppm, respectively, which are used to calculate the degree of polymerization (DP_n) and number-average molecular weight (M_n) (Table 1). The M_n obtained by SEC deviates from that of ^{1}H NMR, which is attributed to the difference between the resulting polymer and standard sample. However, the SEC trace of PHFBMA (Figure 1B) shows a low dispersity and a typical symmetric singlet without a shoulder peak, demonstrating the controllability and "livingness" of this polymerization. Cu(0)-mediated RDRP suffers from a drawback of relatively long induced time. During this period, long polymer chains and high polydispersity can be observed.[52] According to our previous simulation work,[51] a small mount deactivator was added to the reaction system, which had a positive effect on the polymerization. The pseudofirst order kinetics in the semilogarithmic kinetic plot depicted in Figure 2A is linear during HFBMA polymerization, indicating that the time needs to attain ATRP equilibrium is shortened. No obvious induced period and long polymer chain formation are observed at the early stage of polymerization as confirmed by the low dispersity (<1.2).

Subsequently, polymerization of *t*BA using PHFBMA-Cl macroinitiator was carried under similar conditions. The ^{1}H NMR spectrum (green) in Figure 1A confirms the successful incorporation of *t*BA monomer in polymer chains. The characteristic peaks for the protons of tertiary butyl located at 1.35–1.55 ppm and the protons of methyne in acrylate main chain located at 2.10–2.40 ppm are clearly observed. The DP_n of *t*BA can be achieved through calculating the ratio of the integral area of the methyne protons (peak e) in acrylate main chain and that of hexafluorobutyl methacrylate (peak d). Similarly, the kinetic plot illustrated in Figure 2B is used to monitor the health status of the chain extension reaction. The semilogarithmic concentration increased linearly with the time, with a dispersity as low as 1.3. Both results meet the criteria of successful Cu(0)-mediated RDRP. Based on the kinetic study, block copolymers with different P*t*BA segment lengths were prepared by predetermining the reaction time. In this study,

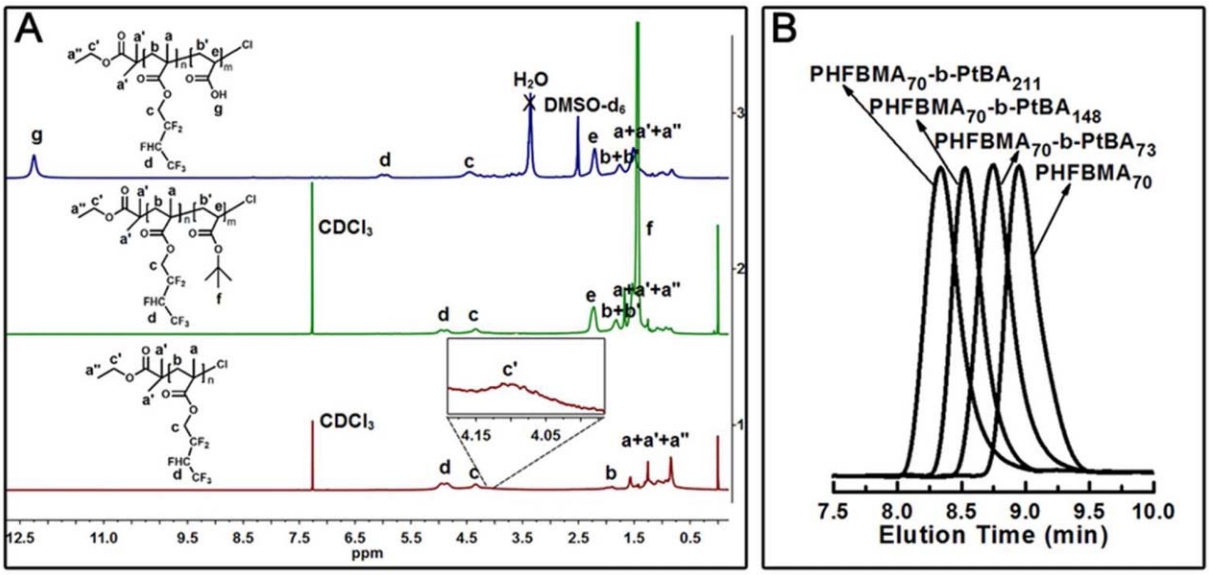

Figure 1. (A) ^{1}H NMR spectra of PHFBMA-Cl (red), PHFBMA-*b*-P*t*BA (green), and PHFBMA-*b*-PAA (blue); (B) SEC traces of PHFBMA-Cl and blcok copolymers with different P*t*BA segment lengths.

[Color figure can be viewed in the online issue, which is available at wileyonlinelibrary.com.]

the ratios of the integral area shown in Supporting Information Figure S1 indicate that the resulting block copolymers have a P*t*BA chain length from 73 to 211. The molecular weights of these block copolymers, ranging from 30400 g/mol to 52100 g/mol, were prepared as summarized in Figure 1B and Table 1.

Finally, the successful deprotection of the tertiary butyl group into a carboxylic acid group was confirmed by ^{1}H NMR analysis, showing a significantly weakened signal at 1.35–1.45 ppm, fixed signals at 2.10–2.40 ppm and 4.20–4.40 ppm, and an intense peak at 12.00–12.45 ppm. The shift of methyne protons (-C*H*F-) from 4.70–5.20 ppm to 5.80–6.15 ppm is attributed to the use of different deuterated reagents. Directly measuring M_n of PHFBMA-*b*-PAA and its dispersity through SEC is difficult because of a large number of carboxylic acid polar groups in the copolymer. The M_ns listed in Table 1 were acquired by indirect calculation from those of PHFBMA-*b*-P*t*BA. Thus far, three pH-responsive block copolymers with well-defined structure were prepared and used for the following studies.

Thermal property of polymers

The block copolymer consists of two or more chemically heterogeneous segments through connection of covalent bonds, showing different properties (e.g., glass transition behavior) from homopolymer, random, and gradient copolymers.[42] Thermal analysis was performed by DSC to trace the thermal properties of the resulting polymers. Figure 3A shows the results for the fluorinated homopolymer and three PHFBMA-*b*-P*t*BA block copolymers. PHFBMA has one clear glass transition region with $T_g = 46.8\,^\circ$C at midpoint of heat capacity change. After introducing the second block through chain extension of PHFBMA, two discernible glass transition regions assigned to P*t*BA and PHFBMA are observed at 37.8 °C and 50.1 °C in PHFBMA$_{70}$-*b*-P*t*BA$_{73}$, respectively. The relatively higher T_g for the PHFBMA domain compared with its homopolymer is attributed to the result of the incompatibility between the two segments. However, only one region for both block copolymers with longer P*t*BA block length (PHFBMA$_{70}$-*b*-P*t*BA$_{148}$ and PHFBMA$_{70}$-*b*-P*t*BA$_{211}$) is found in their own DSC heating curves; their T_gs are reported in Table 1. One rational reason for this finding is the overlapping of the glass transition regions for the P*t*BA and PHFBMA domains. As we all know, the values for the T_g of polymer can be affected by its stereoregularity and molecular weight. As a consequence, the values for the T_g of P*t*BA cover a range from 37 °C to 45 °C.[53–55] Herein, the increase in P*t*BA segment length (higher M_n) leds to the enlargement of the glass

Table 1. Summary of Resulting Polymers

Polymers	$M_{n,NMR}$ (g mol^{-1})	$M_{n,SEC}$ (g mol^{-1})	M_w/M_n (SEC)	T_{g1} (°C)	T_{g2} (°C)
PHFBMA$_{70}$	17500	20200	1.15	46.8	N/A
PHFBMA$_{70}$-*b*-P*t*BA$_{73}$	26900	30400	1.22	35.7	50.1
PHFBMA$_{70}$-*b*-P*t*BA$_{148}$	36500	41700	1.19	36.2	N/A
PHFBMA$_{70}$-*b*-P*t*BA$_{211}$	44600	52100	1.21	42.3	N/A
PHFBMA$_{70}$-*b*-PAA$_{73}$	22800[a]	N/A	N/A	47.2	94.7
PHFBMA$_{70}$-*b*-PAA$_{148}$	28200[a]	N/A	N/A	47.8	101.0
PHFBMA$_{70}$-*b*-PAA$_{211}$	32700[a]	N/A	N/A	51.0	118.0

[a]the M_n was calculated according to the equation

$$M_{n,NMR}(\text{PHFBMA}_{70}-b-\text{PAA}_m) = M_{n,NMR}(\text{PHFBMA}_{70}) + m \cdot \overline{M}(\text{AA});$$

m is the average polymerization degree of PAA and equals to that of P*t*BA

$$\overline{M}(\text{AA}) = 72 \text{ g/mol}.$$

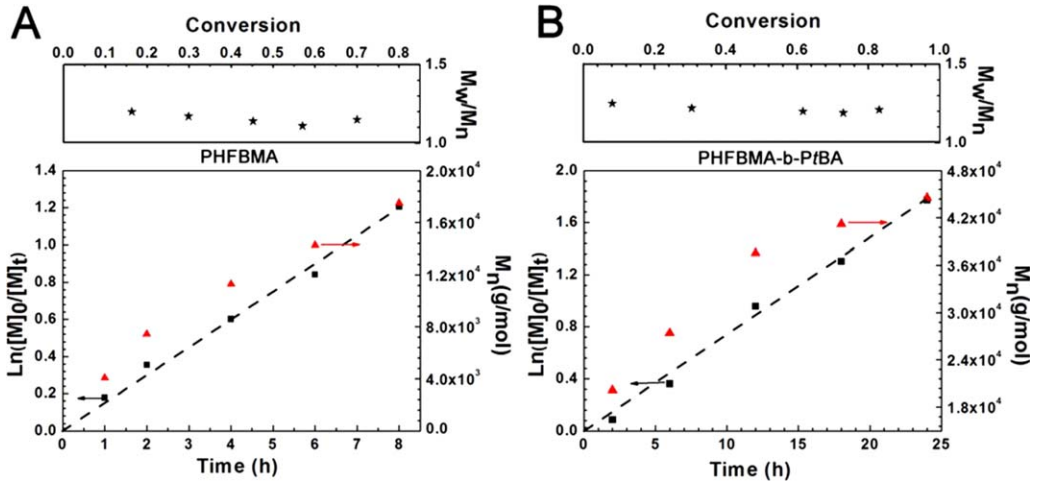

Figure 2. Semilogarithmic kinetic plot, evolution of M_n with time, and evolution of M_w/M_n with conversion for the polymerization of HFBMA (A) and *t*BA (B).

[Color figure can be viewed in the online issue, which is available at wileyonlinelibrary.com.]

transition region approaching the corresponding PHFBMA region, thereby allowing these two regions overlap. A significant evidence on the increase in $T_{g,PtBA}$ is the right-shift of the onset temperature of the glass transition regions.

The characterization of T_gs for the three PHFBMA-*b*-PAA block copolymers is depicted in Figure 3B. Relative to the PHFBMA-*b*-P*t*BA block copolymer, PAA-containing block copolymers have two distinct T_gs that correspond to the PHFBMA and PAA blocks because of the considerable difference in the thermal property between the PHFBMA and PAA segments. With the increase in PAA segment length, the T_g associated to the PAA domain increased from 94.7 °C to 118.0 °C. This result is in consistent with the T_g value range (88–148 °C) as has been reported previously.[56–58] In addition, the slight increase in the onset temperature of the glass transition regions and T_g responses for the PHFBMA domains in block copolymers is influenced by the higher T_g of PAA. After carefully examining the thermal property of the resulting polymers, we further confirmed that the well-defined pH-responsive block copolymers were prepared successfully.

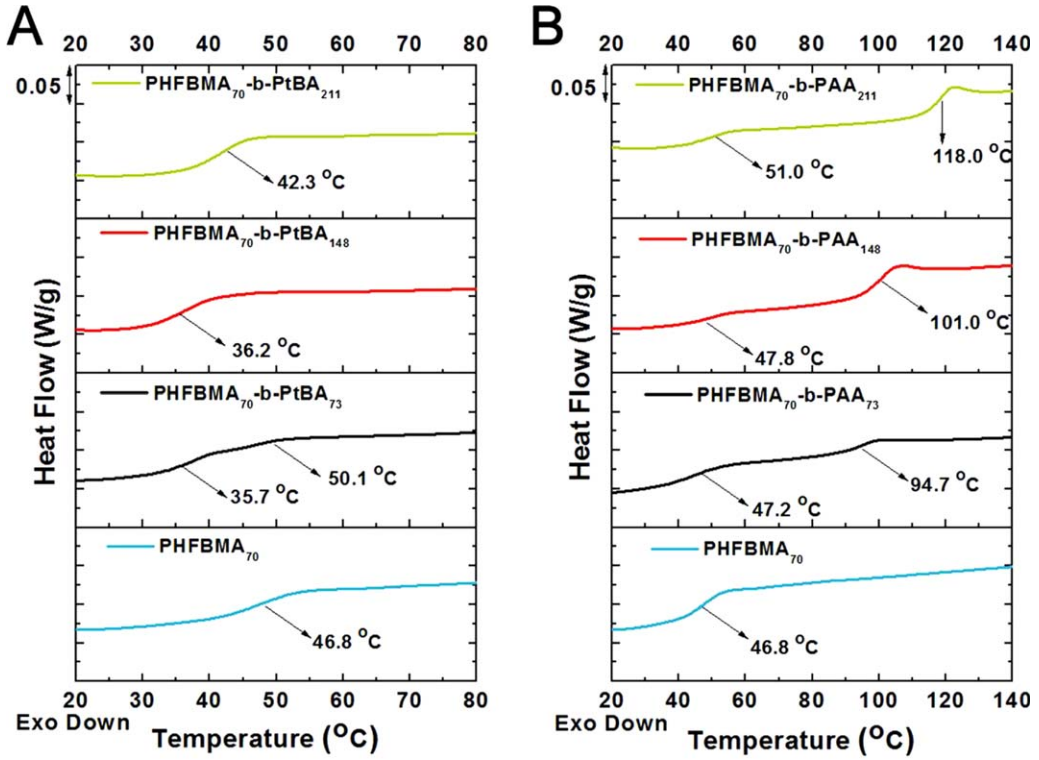

Figure 3. (A) DSC heating curves for $PHFBMA_{70}$ and PHFBMA-*b*-P*t*BA blcok copolymers with different P*t*BA segment lengths, (B) DSC heating curves for $PHFBMA_{70}$ and PHFBMA-*b*-PAA blcok copolymers with different PAA segment lengths.

[Color figure can be viewed in the online issue, which is available at wileyonlinelibrary.com.]

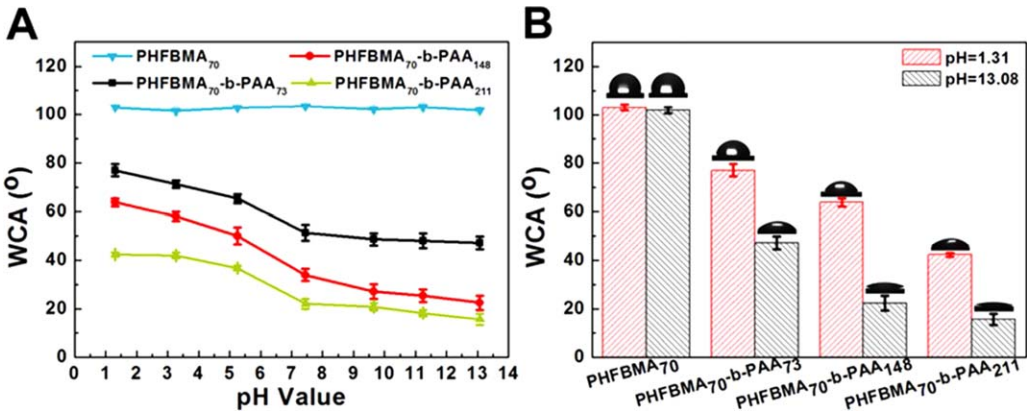

Figure 4. (A) Evolution of WCA with pH (the reported angles are statistically analyzed using three readings from different locations) and (B) representative WCA images for the silicon wafer coated with $PHFBMA_{70}$ and PHFBMA-*b*-PAA blcok copolymers with different PAA segment lengths.

[Color figure can be viewed in the online issue, which is available at wileyonlinelibrary.com.]

pH-responsive wettability of as-prepared surface

Interests in understanding and regulating surface wettability based on stimuli-responsive polymer have persisted in recent years. Commonly, the wetting properties of smooth solid surfaces are described by a Young's equilibrium contact angle.[59] Given the real study systems, apparent static contact angles or dynamic contact angles (known as advancing and receding angles), are generally measured and used to characterize rough surface wetting behaviors due to its heterogeneity.[60] According to the theoretical model proposed by Tadmor, equilibrium contact angle can be obtained indirectly through an expression relating advancing and receding contact angles of rough surface for in-depth investigating intrinsic wettability of as-fabricated surfaces.[61] In this study, pH-responsive wettability of the surfaces spin-coated by PHFBMA-*b*-PAA block copolymers with different PAA segment lengths were investigated using apparent static contact angles.

The pH-dependent wettability of the as-prepared surfaces was studied by dropping the water droplet with different pH values from 1.31 to 13.08. As shown in Figure 4A, the water contact angle (WCA) for the surface coated with PHFBMA film maintains at about 105.0° with slight fluctuation over the testing range. This result indicates that the PHFBMA film is hydrophobic and its wettability is not affected by the pH of the probe liquid. By contrast, the surfaces coated with three block copolymers become hydrophilic and exhibit a pH-responsive wetting characteristic. Furthermore, three interesting phenomena are found after comparing these pH-responsive surfaces. First, the hydrophilicity at acidic (pH = 1.31) and at basic (pH = 13.08) conditions is enhanced by increasing the PAA block length from 73 to 211, as demonstrated in Figure 4B. This result indicates that the deprotonated carboxyl groups with intermolecular hydrogen bond between carboxylic acid moieties and water molecules are more hydrophilic than those protonated carboxyl groups with intramolecular interaction of carboxylic acid groups. Second, the difference of WCA between acidic condition and basic condition shows a maximum value ($\triangle$WCA $\approx$ 40°) for the surface coated by $PHFBMA_{70}$-*b*-PAA_{148}. The other surfaces have similar $\triangle$WCA of 30°, but completely different mechanisms. The reason for the surface coated with $PHFBMA_{70}$-*b*-PAA_{73} is its lower PAA content, whereas the limitation of the $PHFBMA_{70}$-*b*-PAA_{211} surface is caused by its pronounced hydrophilicity at acidic condition. Third, all the three evolutions of WCA with pH share a similar inflection point at pH 5.25, which is higher than the pKa of PAA obtained in the aqueous solution. This result implies that the acidity of carboxylic acid on surface is lower than that of its aqueous solution, which is attributed to the decrease in dielectric constant and hindrance on the intermolecular hydrogen bond caused by the existence of the methyl and fluotinated moieties in PHFBMA block.[5] Thus, the length of the PAA block has a significant influence on controllable surface wettability.

In addition to the controllable wetting behavior, the reversibility of the pH-responsive surfaces was also studied. The pH-responsive wetting property of the samples is recovered by rinsing them with deionized water and then drying with nitrogen flow. As summarized in Figure 5, the repeatedly cyclic tests at different pH values show that all the surfaces exhibit a good transformation of wettability within five cycles. The reported WCAs for each surface were repeatable and stable.

Surface morphology and composition

As known to all, wettability of solid surfaces is regulated by the surface morphology and composition.[62] The morphologies

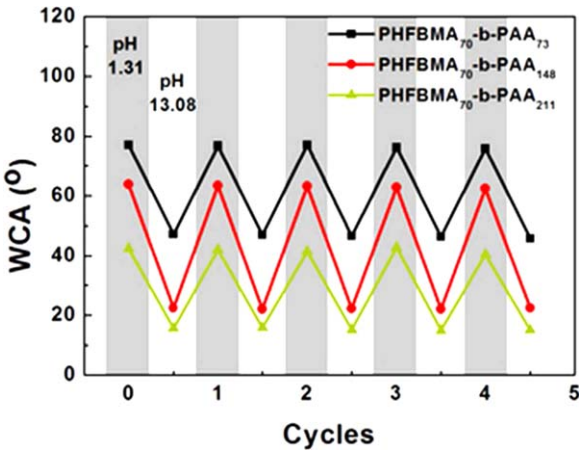

Figure 5. Reversible water wettability of the as-fabricated surfaces coated with PHFBMA-*b*-PAA blcok copolymers with different PAA segment lengths at different pH.

[Color figure can be viewed in the online issue, which is available at wileyonlinelibrary.com.]

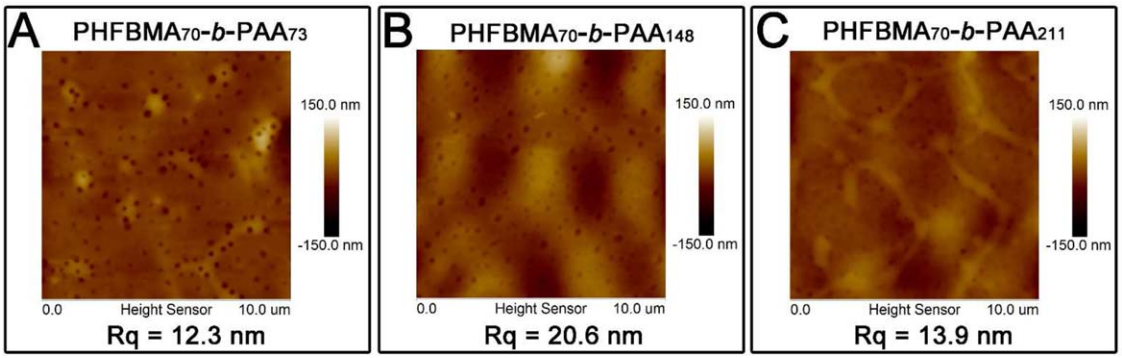

Figure 6. AFM images of the surfaces coated with different block copolymers.

(A) PHFBMA$_{70}$-*b*-PAA$_{73}$, (B) PHFBMA$_{70}$-*b*-PAA$_{148}$, and (C) PHFBMA$_{70}$-*b*-PAA$_{211}$. [Color figure can be viewed in the online issue, which is available at wileyonlinelibrary.com.]

of the surfaces spin-coated with different block copolymer films were scanned by AFM. The typical images are shown in Figure 6, which are similar to all samples. The root-mean-square roughness (Rq) of the coated surfaces is 12.3 nm for PHFBMA$_{70}$-*b*-PAA$_{73}$, 20.6 nm for PHFBMA$_{70}$-*b*-PAA$_{148}$, and 13.9 nm for PHFBMA$_{70}$-*b*-PAA$_{211}$, respectively. No distinguished difference in roughness is observed, indicating that the different wetting properties of the as-prepared surfaces mainly stem from the change in surface composition.

To further study the wetting behavior of the as-prepared surfaces, surface composition was detected by XPS as shown in Figure 7. Figure 7A depicts the survey scan spectra with similar peak shifts for the three surfaces, which centre at 285 eV for C1s, 531 eV for O1s, and 689 eV for F1s.[43] However, the surface content of fluorine decrease and oxygen increase with the increase in PAA block length based on the element ratios listed in Table 2. Surface enrichment of fluorinated moieties is observed in all of three samples, resulting from the low-surface energy of fluorine.

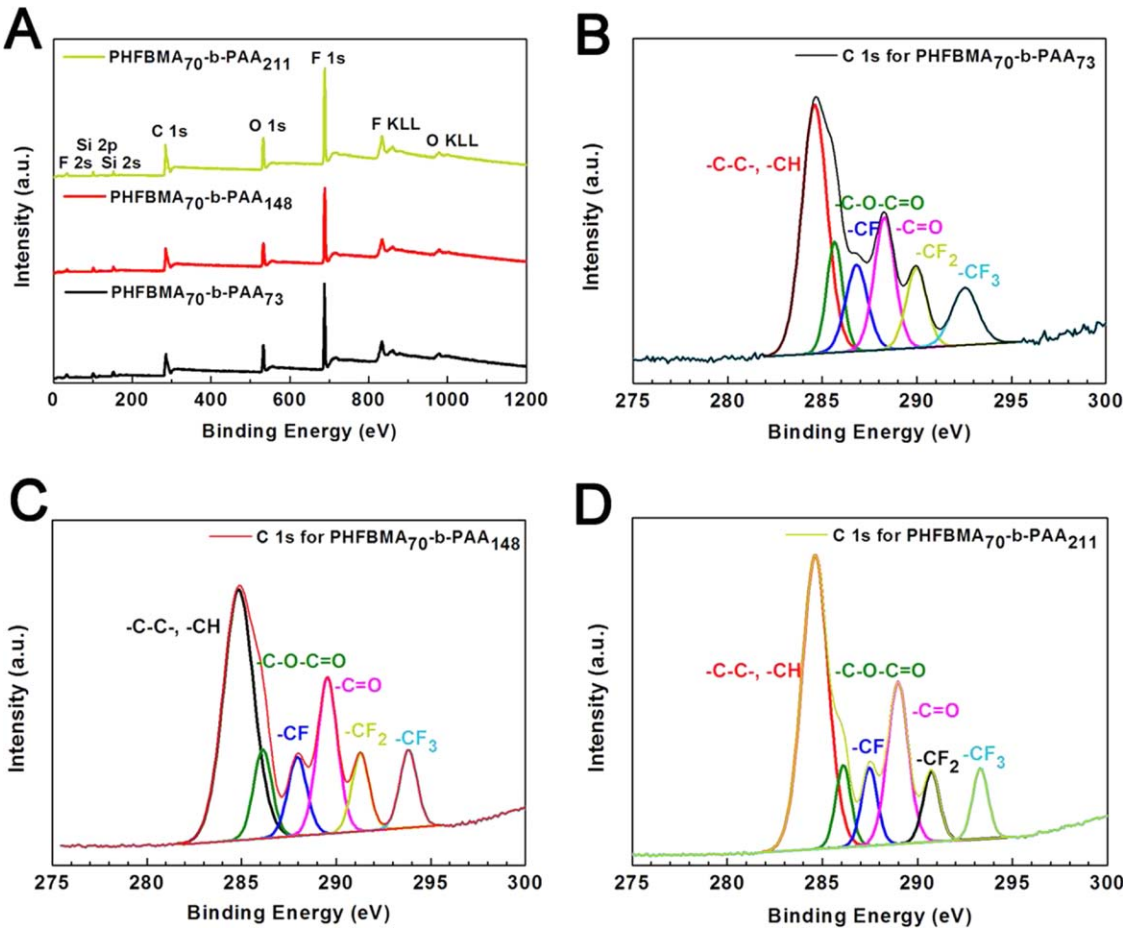

Figure 7. XPS spectra results of the surfaces coated with different block copolymers.

(A) survey scan spectra, (B) high resolution C 1s spectrum for PHFBMA$_{70}$-*b*-PAA$_{73}$, (C) high resolution C 1s spectrum for PHFBMA$_{70}$-*b*-PAA$_{148}$, and (D) high resolution C 1s spectrum for PHFBMA$_{70}$-*b*-PAA$_{211}$. [Color figure can be viewed in the online issue, which is available at wileyonlinelibrary.com.]

Table 2. Surface Composition of the Surfaces Coated with Different Polymers[a]

Polymers[b]	Element Ratio		Surface Composition of Carbon-Based Groups (%)					
	F1s/C1s	O1s/C1s	-C-C-/-CH	-C-O-C=O	-CF	-C=O	$-CF_2$	$-CF_3$
$PHFBMA_{70}$-*b*-PAA_{73}	0.40 ± 0.02	0.23 ± 0.01	39.9 ± 2.0	11.2 ± 0.4	11.9 ± 0.6	17.2 ± 0.9	10.2 ± 0.3	9.6 ± 0.2
$PHFBMA_{70}$-*b*-PAA_{148}	0.37 ± 0.01	0.24 ± 0.01	45.9 ± 2.3	9.8 ± 0.5	9.1 ± 0.4	18.9 ± 0.8	8.2 ± 0.3	8.1 ± 0.3
$PHFBMA_{70}$-*b*-PAA_{211}	0.36 ± 0.02	0.25 ± 0.01	48.8 ± 2.1	7.9 ± 0.4	7.8 ± 0.3	21.2 ± 1.0	7.4 ± 0.2	6.9 ± 0.2

[a]The reported values are statistically analyzed using three results from every sample.
[b]Bulk composition (mass fraction) of F element is 35.0% for $PHFBMA_{70}$-*b*-PAA_{73}, 28.3% for $PHFBMA_{70}$-*b*-PAA_{148}, 24.4% for $PHFBMA_{70}$-*b*-PAA_{211}.

The high resolution C1s spectrum with complex pattern was resolved into six well-fitted Gauss peaks to access the composition of carbon-based groups at different surfaces. The fitting peaks centre at 284.8, 285.4, 287.8, 288.9, 290.8, and 292.7 eV are assigned to -C-C-/-C-H, -C-O-C=O, -CF, -C=O, $-CF_2$, and $-CF_3$ eV, respectively. These peaks are clearly observed in Figures 7B–D and agreed with the related bonding energies of the functional group in the block copolymer as confirmed by previously works.[44,63,64] The composition proportion results shown in Table 2 indicate that the contents of the -CF, $-CF_2$ and $-CF_3$ groups at the topmost surface decrease with the decrease in bulk composition of the fluorinated moieties. Meanwhile, the surface contents of the -C=O group increase with the increase in PAA block length. The different surface compositions provide the rational explanations for the different wetting behaviors observed above. For example, the surface coated by $PHFBMA_{70}$-*b*-PAA_{73} has the highest proportion of fluorinated group and lowest proportion of carbonyl group, which can be taken into account for its poor hydrophilicity.

Wettability of coated stainless steel mesh surface

Oil-polluted water as one of the serious environmental issues has received considerable attention. Functional polymeric materials with special wettability have a potential in efficient water/oil separation.[65] The block copolymers synthesized in this work with good hydrophilicity would be good candidates for separating a layered water and oil mixture. By directly casting the polymer solution onto a SSM, a polymer-coated mesh can be obtained and used for water/oil separation. It is worth noting that the proposed method is rather simple and effective as has been confirmed before.[15,18,66–72]

In this study, the initial SSM is knitted by metal wires with average square-shaped pore size of 45 μm as shown in Supporting Information Figure S2. The water and underwater oil contact angles of the initial SSM were measured and used as a reference for the coated SSMs. The WCAs at acidic and basic condition are 123° and 121°, respectively; the underwater oil CAs at acidic and basic condition are 116° and 117°, respectively. The results show that the water/oil wettability of non-coated SSM is hydro-/oleo-phobic and is not affected by the pH conditions. Compared with the noncoated SSM, the coated SSMs are covered with homogeneous block copolymer films and without obvious defect as depicted in the left panel of Figure 8. And also, the average diameter of the knitted metal wires increases from ~35 μm to ~40 μm (40.3 μm for $PHFBMA_{70}$-*b*-PAA_{73} film, 40.1 μm for $PHFBMA_{70}$-*b*-PAA_{148} film and 40.5 μm for $PHFBMA_{70}$-*b*-PAA_{211} film) after solution casting. Furthermore, the magnified images (Supporting Information Figure S3) show that the honeycomb microstructure of the copolymer film over the coated SSM is clearly observed in all samples, which is ascribed to the solvent evaporation. The rough microstructure and knitted network structure will enhance the water/oil wettability of the as-prepared SSMs.

Contact angle measurements were also performed to probe the wetting properties of the coated SSMs. For the SSM coated with $PHFBMA_{70}$-*b*-PAA_{73} film, the CA of an acidic water droplet (pH = 1.31) is 116° (Figure 8A, middle panel), indicating that the surface is hydrophobic. Even at basic condition (water drop with pH = 13.08), the surface with a WCA of 88° (Figure 8A, right panel) shows a poorer hydrophilicity than that of the flat substrate as shown in Figure 4. These results should be ascribed to the synergistic effect of the surface chemical composition and roughness. The higher fluorinated moiety content and the Cassie-Baxter model with entrapped air in the groove structures underneath the water droplet forming a composite interface of air and solid[73] cause the loss of surface hydrophilicity.

The water wettability of the SSMs coated with $PHFBMA_{70}$-*b*-PAA_{148} and $PHFBMA_{70}$-*b*-PAA_{211} films is significantly enhaced in air as demonstrated in Figures 8B and 8C. Taking the results of the two samples on polymer-based silicon surfaces as references (Figure 4), the present phenomena can be properly described by the Wenzel theory,[74] which recognizes that hydrophilicity can be significantly amplified on a rough surface indicating a water droplet pinned to the rough surface. At acidic condition, the WCA of the $PHFBMA_{70}$-*b*-PAA_{148} film is 18°, whereas 0° for $PHFBMA_{70}$-*b*-PAA_{211} film surface, which is attributed to the different PAA chain lengths. However, this result should not influence the practical application as will be discussed below. Furthermore, when a basic water droplet (pH = 13.08) is applied to both surfaces, the droplet spreads out immediately, indicating that these surfaces are both superhydrophilic. The intense interaction between base and acid on the liquid-soild interface allows the surface to be wetted rapidly by increasing the contact area of the droplet and the surface. Given that the as-prepared SSMs exhibit excellent water retention capacity (hydrophilicity or even superhydrophilicity) independent of the pH of the aqueous solution in air, they can repel the oil effectively when separating the water and oil mixture. The schematic illustration of the water wettability of the block copolymer-coated SSM and the model of the oil repelled state are shown in Scheme 2.

Underwater oil wettability is an important issue that affects the working life of the separation mesh.[65] Underwater oil CA measurements were conducted to examine the oil wetting behaviors of the coated surfaces in the aqueous solution with different pH. In this study, the underwater oil (hexane) wetting behaviors at acidic and basic conditions illustrate that the surface coated with $PHFBMA_{70}$-*b*-PAA_{73} film is oleophobic. The difference between oil CA in acidic water and basic water is attributed to the different hydrophilic properties (in other words, different water retention capacities) of protonated and deprotonated PAA chains. The existence of underwater oleophilic PHFBMA chain and the collapsed PAA chain

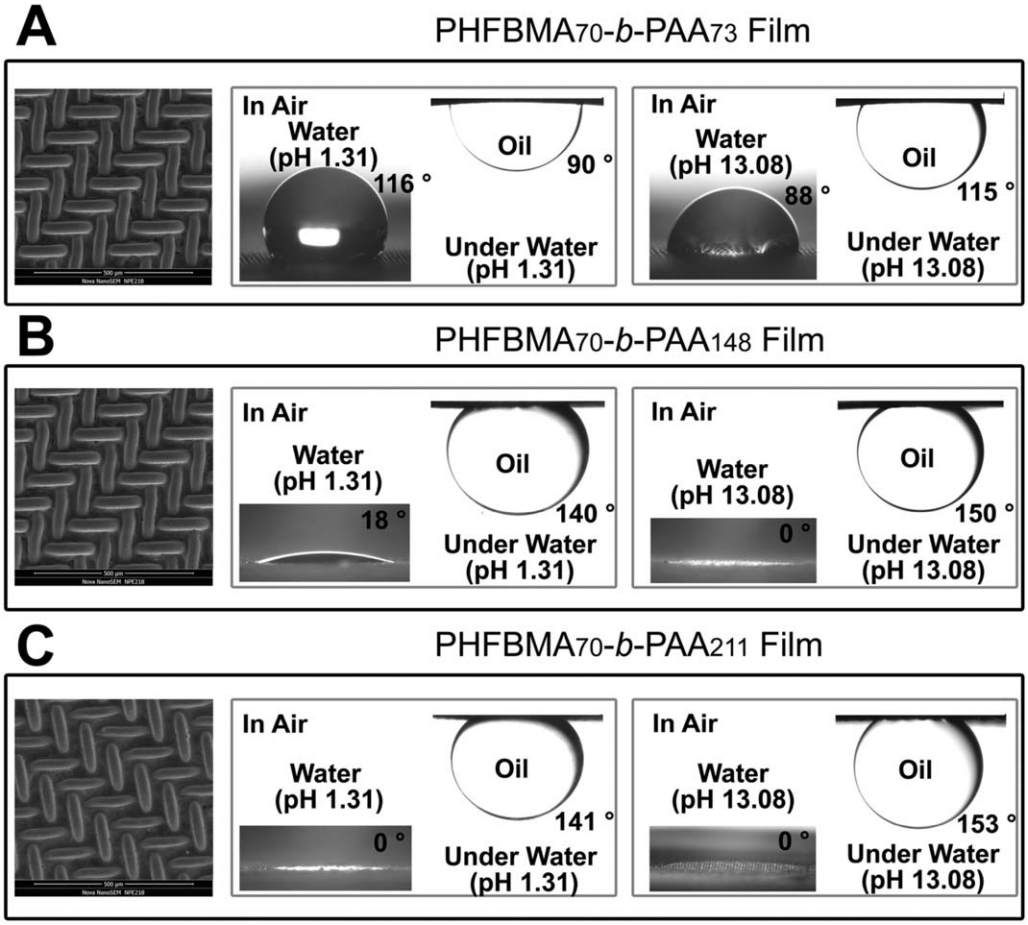

Figure 8. SEM images (left panel, scale bar is 500 μm), water/oil (hexane) wettability at acidic condition (middle panel), and water/oil wettability at basic condition (right panel) of the SSMs coated with different block copolymers.

(A) PHFBMA$_{70}$-*b*-PAA $_{73}$ film coated SSM, (B) PHFBMA$_{70}$-*b*-PAA$_{148}$ film coated SSM, (C) PHFBMA$_{70}$-*b*-PAA$_{211}$ film coated SSM.

conformation under acidic water leads to lower water content and higher oil adhesion of the surface.[25] By contrast, the surface oleophobicity is enhanced because of the stretched PAA chain conformation with higher water content in the basic environment.

As shown in Figures 8B, C, the underwater oil CAs of about 140° are obtained in acidic water for both block copolymer films, which increase to about 150° at basic condition, indicating the superoleophobicity of the as-prepared SSMs. As discussed previously, the basic surrounding environment allows the PAA chains to dissociate and form intermolecular hydrogen bonding with water molecules, making the SSMs have extremely high water retention capacity. The stable water layer prevents the oil from wetting the SSMs effectively, leading to their superoleophobicity. Meanwhile, the protonated PAA segments are collapsed because of the intramolecular hydrogen bonding in acidic solution. As a result, the water content kept in the coated SSMs decreases; hence the oil droplet approaches the polymer-coated surface, affording it with high oil adhesion. Scheme 2 demonstrates the pH induced switchable oil wettability under water. Notably, the underwater oil repellency of the SSMs coated with PHFBMA$_{70}$-*b*-PAA$_{148}$ and PHFBMA$_{70}$-*b*-PAA$_{211}$ films are much higher than that of the PHFBMA$_{70}$-*b*-PAA$_{73}$ film-coated SSM. This result is ascribed to the fact that the block copolymer with long PAA chains can avoid the oleophilic PHFBMA chains from interacting with the oil droplet. Such good oil repellency can maintain efficient and stable separation for a long time.

Application of the coated SSMs to water/oil separation

Understanding the mechanism of the wetting behaviors of the as-prepared SSMs, a separation device was fabricated for water/oil separation as a proof of concept. A pre-wetted coated SSM with effective filtration area of 0.96×10^{-3} m^2 was fixed in the middle of the filter, and a conical flask was placed at the bottom to collect the permeated liquid (Figure 9A). The prewetting process endows the coated SSM with stable superoleophobicity by trapping abundant water into the superhydrophilic copolymer film. As shown in the left panel of Figure 9A, a mixture of layered n-hexane and water (1:1, v/v) is poured into the filter. The water can selectively pass through the coated SSM driven only by gravity, whereas the n-hexane is blocked at the upper container (right panel of Figure 9A). In addition, the used SSMs can be recycled by simply water cleaning and nitrogen flow drying. The separation of the water and oil mixture is depicted schematically in Scheme 2. The trapped water acts as a barrier to repel the oil and permit water to percolate through the coated SSM.

In our study, three coated SSMs were utilized to separate a n-hexane/water (pH 1.3/7.0/13.1) mixture with 1:1 volume

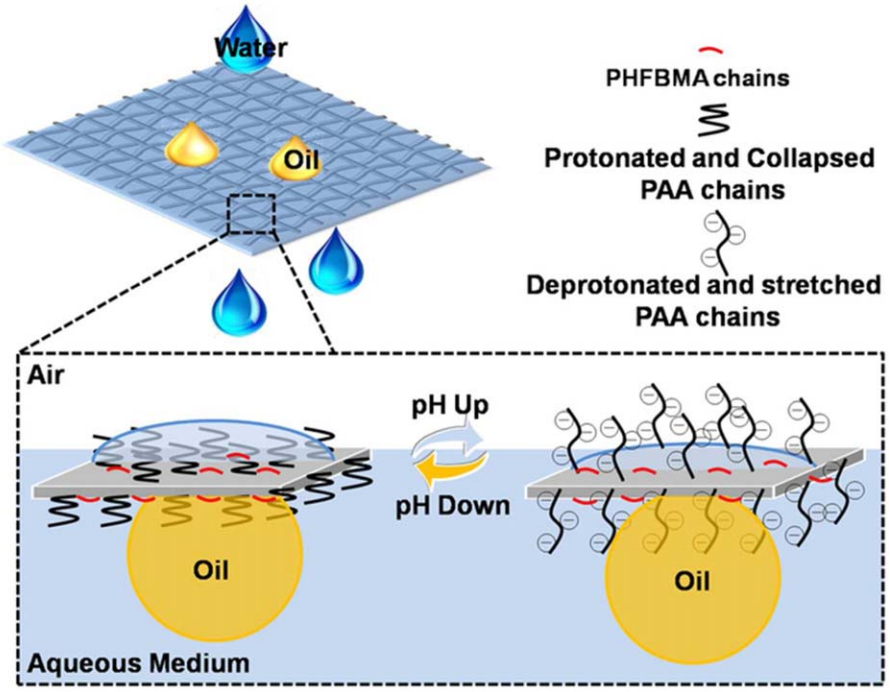

Scheme 2. The schematic illustration of the water in air and the oil under water wettability of the block copolymer-coated SSM.

[Color figure can be viewed in the online issue, which is available at wileyonlinelibrary.com.]

ratio and subsequently identify a better candidate for efficient separation. As for the prewetted $PHFBMA_{70}$-*b*-PAA_{73} coated SSM, the mixtures with water (pH 1.3/7.0/13.1) can hardly flow through the mesh due to its poor hydrophilicity. Whereas, the separations of water with pH 1.3, pH 7.0 or pH 13.1 from the mixtures using prewetted $PHFBMA_{70}$-*b*-PAA_{148} coated SSM and $PHFBMA_{70}$-*b*-PAA_{211} coated SSM perform smoothly with similar feature. The results were summarized in Supporting Information Table S1. Results show that the water flux is not in response to pH obviously. Given comparing with other opened reports conveniently, the following study was performed using the mixture (200 mL) with water (pH 7.0). All of the separation processes were recorded and provided as Supporting Information Video S1, Video S2, and Video S3. No visible oil was observed in the filtered water. The water fluxes of the SSMs are obtained by measuring the time needed to collect a certain volume of water (pH 7.0). The representative results are listed in Figure 9B, where shows the flux is 0.12 L s^{-1} m^{-2} for the $PHFBMA_{70}$-*b*-PAA_{73} coated SSM, 10.21 L s^{-1} m^{-2} for $PHFBMA_{70}$-*b*-PAA_{148} coated SSM, and 10.42 L s^{-1} m^{-2} for $PHFBMA_{70}$-*b*-PAA_{211} coated SSM. Obviously, the poor water wettability as confirmed previously leads the SSM coated with the copolymer with low PAA content to exhibit a distinct disadvantage in separation performance. By contrast, because of their superhydrophilicity and underwater superoleophobicity, the other two SSMs have excellent separation performances with a similar flux of about 10 L s^{-1} m^{-2}. Importantly, the

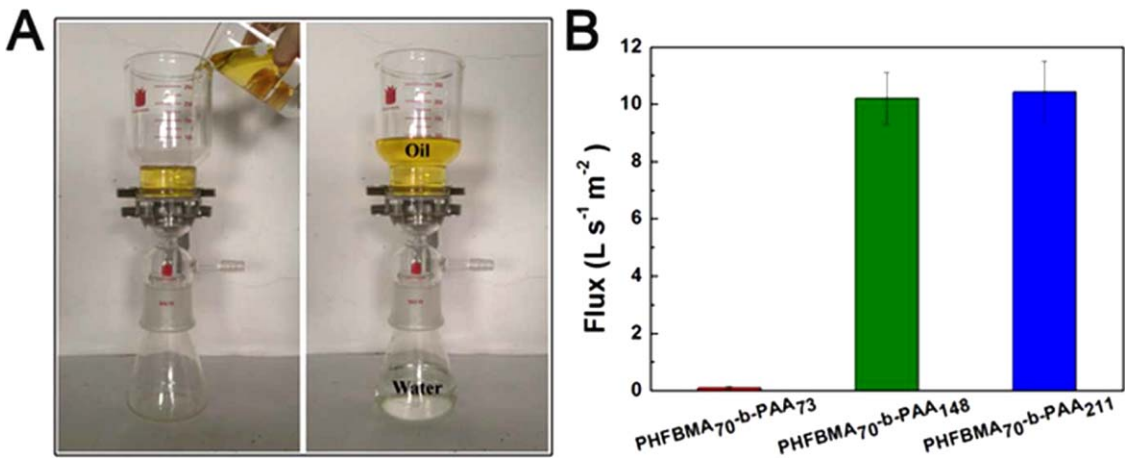

Figure 9. (A) Separation setup and process. Water flows through the coated SSM (left panel) and n-hexane is dyed yellow by ferrocene and retains at the upper container (right panel), (B) Water fluxes of the coated SSMs (The reported values are statistically analyzed using three different samples).

[Color figure can be viewed in the online issue, which is available at wileyonlinelibrary.com.]

Table 3. Comparison Between some Advanced Separation Membranes

Chemical Composition	Type	Water Flux ($L\ s^{-1}\ m^{-2}$)	References
PHFBMA-b-PAA	Solution-cast SSM with pore size of 45 μm	10.4	This work
Polyacrylamide	Hydrogel-coated SSM with pore size of 50 μm	17.5	66
A mixture of aqueous poly(diallyldimethylammonium chloride) solution, sodium perfluorooctanoate, and silica nanoparticles	Spray-coated SSM with pore size of 200 μm	Not Given	67
Poly(diallyldimethylammonium chloride), sodium silicate and TiO_2 nanoparticles	Dip-coated SSM with pore size ranging from 180 μm	Not Given	68
A mixture of aqueous poly(diallyldimethylammonium chloride) solution, sodium perfluorooctanoate, and silica nanoparticles	Dip-coated SSM with pore sizes ranging from 42 to 60 μm	0.48	69
Poly(styrene-co-maleic anhydride) fluorosurfactant complex solution	Dip-coated SSM with pore size of 200 μm	Not Given	70
Poly (N,N-dimethylaminoethyl methacrylate)	Hydrogel-coated SSM with pore size of 40 μm	Not Given	18
$Cu(OH)_2$	Nanowire-haired Copper mesh with pore sizes ranging from 25 to 75 μm	0.14–44.0	71
Graphene oxide	Dip-coated SSM with pore size of 40 μm and 50 μm	10.0 and 22.0	72
$CaCO_3$-based commercial polypropylene membrane grafted with poly(acrylic acid)	Microporous membrane with pore sizes ranging from 200 to 750 nm	0.56	75
Commercial nitrocellulose membrane	Perforated membrane with micro-sized pore ranging from 49 to 133 μm	0.85–9.5	76
Poly(methyl methacrylate)-co-poly(N,N-dimethylaminoethyl methacrylate)	Electrospun fiber membrane	2.65	19
poly(methyl methacrylate)-b- poly(4-vinylpyridine)	Electrospun fiber membrane	2.61	77
TiO_2-ethanol sol-gel solution	Sol−gel coated natural cotton fabric membrane with pore size of 84 μm	4.72	78
A mixture of silica nanoparticles and heptadecafluorononanoic acid-modified TiO_2 sol	Dip-coated polyester fabric membrane	Not Given	79
Poly(sodium methacrylate) and poly(stearyl methacrylate)	Polymer grafted SSM with pore size of 40 μm	50.0	80

separation performance evaluated by the water flux in this study is comparable with or better than some advanced separation membranes that has been summarized in Table 3.

As for the systems using SSMs coated by polymeric materials, Feng and Jiang et al. reported a highly efficient polyacrylamide hydrogel-coated SSM with water flux of about 17.5 L s^{-1} m^{-2}.[66] Free of hydrogel in the pores ensures the rapid permeation of water through the coated SSM. Recently, a gravity-driven organic-inorganic hybrid membrane with 0.48 L s^{-1} m^{-2} flux was prepared by Yoon et al.[69] By contrast, the water flux can be greatly improved when using SSMs coated by all-inorganic materials, such as $Cu(OH)_2$ and graphene oxide.[71,72] In addition, some other types of membranes were also applied in this field. For example, Xu et al. fabricated a mineral-coated polypropylene membrane with a flux of about 0.56 L s^{-1} m^{-2}.[75] Wang and coworkers prepared dual-scaled porous nitrocellulose membranes with pore size ranging from 49 to 133 μm. Because of the increase in pore size, the flux increased from 0.85 to 9.5 L s^{-1} m^{-2} accordingly.[76] More recently, Yuan and coworkers[19] and Luo and coworkers[77] reported CO_2-induced and pH-induced controllable separation electrospun fiber membranes for separating water from water/oil mixture with fluxes of 2.65 and 2.61 L s^{-1} m^{-2}, respectively. Tian and Zhang et al. produced an underwater self-cleaning membrane based on natural fabric for relatively rapid separation, and its water flux reached 4.72 L s^{-1} m^{-2}.[78] Hozumi and coworkers reported a oil/water separation device allowing to run continuously, and separate large volumes of oily water at high flow rates of about 5 L s^{-1} m^{-2}.[80] These results verify that the block copolymer-coated SSMs developed in this work have promising application in water/oil separation.

In addition, the separation efficiency determined by the weight ratio of water before and after separation for the $PHFBMA_{70}$-*b*-PAA_{148} and $PHFBMA_{70}$-*b*-PAA_{211} coated SSMs is as high as 99% (Figure 10A), which meets the requirements for practical application.[66–72,75–80] Moreover, gravity-driven separations of water (pH 7) from n-heptane/water, n-octane/water, petroleum ether (60–90 °C)/water, and diethyl ether/water mixtures were also investigated. Rapid separation processes were achieved for all cases. As summarized in Figure 10A, the separation processes have high efficiency of over 98%, indicating that the as-prepared SSMs exhibit good oil rejection ability for different organic solvent/water mixtures.

Finally, another important issue concerning whether the coated SSMs can maintain the integrality of morphology after separation should be confirmed. Herein, the SSMs coated with $PHFBMA_{70}$-*b*-PAA_{148} and $PHFBMA_{70}$-*b*-PAA_{211} films were recycled for separation experiment. Figure 10B shows the fluxes of water for both SSMs. The water flux of $PHFBMA_{70}$-*b*-PAA_{148} coated SSM stabilizes around 10 L s^{-1} m^{-2} with minimal flux fluctuation after five cycles. However, a slight increase of the water flux of $PHFBMA_{70}$-*b*-PAA_{211} coated SSM is found after repeating five times, which might be the result of the damage of as-fabricated SSM. A small amount of visible oil in the filtrate observed at fifth cycle confirms the degeneration of the separation ability of $PHFBMA_{70}$-*b*-PAA_{211} coated SSM. This phenomenon becomes serious after another five recycles. However, the $PHFBMA_{70}$-*b*-PAA_{148} coated SSM still maintained its high separation efficiency after the experiment. The morphologies of both SSMs were observed after separation as shown in Supporting Information Figure S4. The result shows that the morphology of the $PHFBMA_{70}$-*b*-PAA_{148} film is maintained, whereas that of the $PHFBMA_{70}$-*b*-PAA_{211} film is broken. The reason for the better stability of the $PHFBMA_{70}$-*b*-PAA_{148} film should be attributed to the synergistic effect of the two blocks of the copolymer.

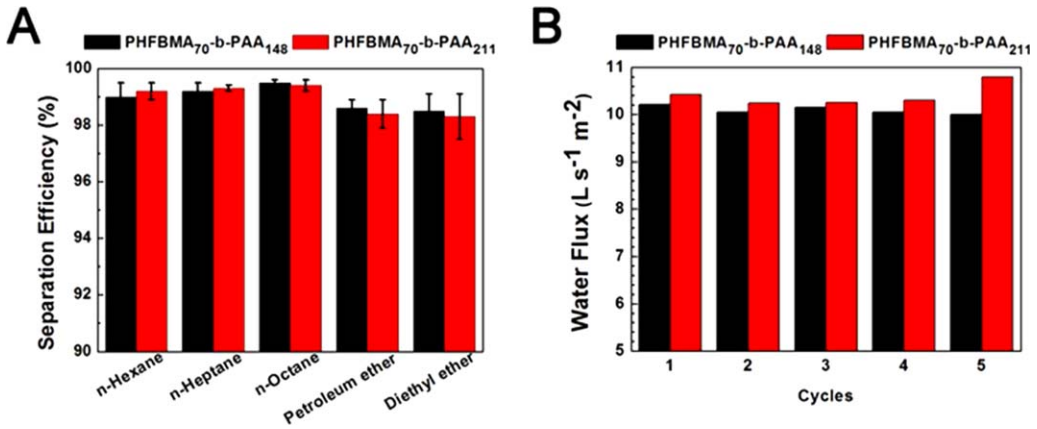

Figure 10. (A) Separation efficiency of the coated SSMs for different organic solvent/water mixtures (100% efficiency means the complete separation of water from the mixture solution; The reported values is statistically analyzed by three different separation processes), (B) Variations in the flux of water for the coated SSMs.

[Color figure can be viewed in the online issue, which is available at wileyonlinelibrary.com.]

That is, the moderate PAA content works for its superhydrophilicy as proven by WCA measurement; the PHFBMA block acts as a physical supporter because of the independence of its own properties (nonresponsive wettability and excellent chemical and thermal stability). Increasing the PAA content in PHFBMA$_{70}$-*b*-PAA$_{211}$ film improves the water retention capacity of the film. However, the film becomes quite affinitive to aqueous medium and inevitable to lose its stability.

Conclusions

Three block copolymers with different PAA segment lengths were successfully synthesized by Cu(0)-mediated RDRP and hydrolysis reaction, which were confirmed by ^{1}H NMR characterization, kinetic study, and thermal property analysis.

By spin-coating the resulting block copolymers onto silicon wafers, careful investigations on the flat surface with pH-dependent wettability were performed by evaluating the contact angle of water-droplet with different pH values from 1.31 to 13.08, surface morphology, and surface composition. The results showed that the pH-responsive wetting behavior was introduced by the PAA block, and the responsiveness of the as-fabricated surfaces was greatly influenced by the PAA content. In comparison to PHFBMA$_{70}$-*b*-PAA$_{73}$ film, PHFBMA$_{70}$-*b*-PAA$_{148}$ and PHFBMA$_{70}$-*b*-PAA$_{211}$ films showed an advantage of hydrophilicity. All three evolutions of WCA with pH shared a similar inflection point at pH 5.25, which was higher than the pKa of PAA obtained in the aqueous solution.

A simple solution-casting technique was developed to functionalize the SSMs using the as-prepared block copolymers for layered water/oil mixture separation. Given their superhydrophilicity and underwater superoleophilicity, PHFBMA$_{70}$-*b*-PAA$_{148}$ and PHFBMA$_{70}$-*b*-PAA$_{211}$ coated SSMs could efficiently separate water from different mixtures of organic solvent and water with high flux. However, considering the long-term use, PHFBMA$_{70}$-*b*-PAA$_{148}$ coated SSM with good stability was the best copolymer for water/oil separation. In summary, a coordination of the structure, composition, and functionality is desired to enable a functional material to obtain practical applications.

Overall, the new product presented here can be developed for a hydrophilic surface with pH-sensitivity. Meanwhile, it also offers a sustainable application in efficient water/oil separation based on the viewpoint of chemical product engineering.

Acknowledgments

The authors thank the National Natural Science Foundation of China (No. 21276213, U1462101), the National Ministry of Science and Technology of China (No. 2012CB21500402) and the National High Technology Research and Development Program of China (No. 2013AA032302) for supporting this work. The authors would like to thank Center for Advanced Electronics Materials and Devices.

Literature Cited

1. Cohen Stuart MA, Huck WTS, Genzer J, Müller M, Ober C, Stamm M, Sukhorukov GB, Szleifer I, Tsukruk VV, Urban M, Winnik F, Zauscher S, Luzinov I, Minko S. Emerging applications of stimuli-responsive polymer materials. *Nat Mater*. 2010;9:101–113.
2. Cussler EL, Wei J. Chemical product engineering. *AIChE J*. 2003; 49:1072–1075.
3. Moggridge GD, Costa R, Saraiva PM. Chemical product engineering: an emerging paradigm within chemical engineering. *AIChE J*. 2006;52:1976–1986.
4. Xin BW, Hao JC. Reversibly switchable wettability. *Chem Soc Rev*. 2010;39:769–782.
5. Yu X, Wang Z, Jiang Y, Shi F, Zhang X. Reversible pH-responsive surface: From superhydrophobicity to superhydrophilicity. *Adv Mater*. 2005;17:1289–1293.
6. Sun W, Zhou S, You B, Wu L. Polymer brush-functionalized surfaces with reversible, precisely controllable two-way responsive wettability. *Macromolecules*. 2013;46:7018–7026.
7. Dunderdale GJ, Urata C, Miranda DF, Hozumi A. Large-scale and environmentally friendly synthesis of pH-responsive oil-repellent polymer brush surfaces under ambient conditions. *ACS Appl Mater Interfaces*. 2014;6:11864–11868.
8. Dunderdale GJ, Urata C, Hozumi A. An underwater superoleophobic surface that can be activated/deactivated via external triggers. *Langmuir*. 2014;30:13438–13446.
9. Pei Y, Travas-Sejdic J, Williams DE. Reversible electrochemical switching of polymer brushes grafted onto conducting polymer films. *Langmuir*. 2012;28:8072–8083.
10. Kwon G, Kota AK, Li YX, Sohani A, Mabry JM, Tuteja A. On-demand separation of oil-water mixtures. *Adv Mater*. 2012;24:3666–3671.
11. Groten J, Bunte C, Rühe J, Light-induced switching of surfaces at wetting transitions through photoisomerization of polymer monolayers. *Langmuir*. 2012;28:15038–15046.
12. Abrakhi S, Péralta S, Fichet O, Teyssié D, Cantin S. Poly(azobenzene acrylate-co-fluorinated acrylate) spin-coated films: influence of

the composition on the photo-controlled wettability. *Langmuir*. 2013; 29:9499–9509.
13. Zhou Y-N, Li J-J, Zhang Q, Luo Z-H. Light-responsive smart surface with controllable wettability and excellent stability. *Langmuir*. 2014;30:12236–12242.
14. Zhou Y-N, Li J-J, Zhang Q, Luo Z-H. A novel fluorinated polymeric product for photoreversibly switchable hydrophobic surface. *AIChE J*. 2014;60:4211–4221.
15. Xue B, Gao L, Hou Y, Liu Z, Jiang L. Temperature controlled water/oil wettability of a surface fabricated by a block copolymer: application as a dual water/oil on-off switch. *Adv Mater*. 2013;25: 273–277.
16. Li J-J, Zhou Y-N, Luo Z-H. Thermo-responsive brush copolymers with structure-tunable LCST and switchable surface wettability. *Polymer*. 2014;55:6552–6560.
17. Li J-J, Zhou Y-N, Luo Z-H. Thermal-responsive block copolymers for surface with reversible switchable wettability. *Ind Eng Chem Res*. 2014;53:18112–18120.
18. Cao Y, Liu N, Fu C, Li K, Tao L, Feng L, Wei Y. Thermo and pH dual-responsive materials for controllable oil/water separation. *ACS Appl Mater Interfaces*. 2014;6:2026–2030.
19. Che H, Huo M, Peng L, Fang T, Liu N, Feng L, Wei Y, Yuan J. CO2-responsive nanofibrous membranes with switchable oil/water wettability. *Angew Chem Int Ed*. 2015;54:8934–8938.
20. Chen L, Wang W, Su B, Wen Y, Li C, Zhou Y, Li M, Shi X, Du H, Song Y, Jiang L. A light-responsive release platform by controlling the wetting behavior of hydrophobic surface. *ACS Nano*. 2014;8: 744–751.
21. Zhang H, Hou X, Zeng L, Yang F, Li L, Yan D, Tian Y, Jiang L. Bioinspired artificial single ion pump. *J Am Chem Soc*. 2013;135: 16102–16110.
22. Zhang L, Zhang Z, Wang P. Smart surfaces with switchable superoleophilicity and superoleophobicity in aqueous media: toward controllable oil/water separation. *NPG Asia Mater*. 2012;4:e8.
23. Zhu H, Chen D, Li N, Xu Q, Li H, He J, Lu J. Graphene foam with switchable oil wettability for oil and organic solvents recovery. *Adv Funct Mater*. 2015;25:597–605.
24. Li J-J, Zhou Y-N, Luo Z-H. Smart fiber membrane for pH-Induced oil/water separation. *ACS Appl Mater Interfaces*. 2015;7:19643–19650.
25. Cheng Q, Li M, Yang F, Liu M, Li L, Wang S, Jiang L. An underwater pH-responsive superoleophobic surface with reversibly switchable oil-adhesion. *Soft Matter*. 2012;8:6740–6743.
26. Sarkar D, Somasundaran P. Conformational dynamics of poly (acrylic acid). A study using surface plasmon resonance spectroscopy. *Langmuir*. 2004;20:4657–4664.
27. Horecha M, Senkovskyy V, Synytska A, Stamm M, Chervanyov AI, Kiriy A. Ordered surface structures from PNIPAM-based loosely packed microgel particles. *Soft Matter*. 2010;6:5980–5992.
28. Lawrence DB, Cai T, Hu Z, Marquez M, Dinsmore AD. Temperature-responsive semipermeable capsules composed of colloidal microgel spheres. *Langmuir*. 2007;23:395–398.
29. Colombani O, Ruppel M, Schubert F, Zettl H, Pergushov DV, Müller AH. Synthesis of poly (n-butyl acrylate)-block-poly (acrylic acid) diblock copolymers by ATRP and their micellization in water. *Macromolecules*. 2007;40:4338–4350.
30. Zhou Y-N, Zhang Q, Luo Z-H. A light and pH dual-stimuli-responsive block copolymer synthesized by copper(0)-mediated living radical polymerization: Solvatochromic, isomerization, and "schizophrenic" behaviors. *Langmuir*. 2014;30:1489–1499.
31. Yoo D, Shiratori SS, Rubner MF. Controlling bilayer composition and surface wettability of sequentially adsorbed multilayers of weak polyelectrolytes. *Macromolecules*. 1998;31:4309–4318.
32. Xia F, Feng L, Wang S, Sun T, Song W, Jiang W, Jiang L. Dual-responsive surfaces that switch between superhydrophilicity and superhydrophobicity. *Adv Mater*. 2006;18:432–436.
33. Currie EPK, Sieval AB, Fleer GJ, Stuart MC. Polyacrylic acid brushes: surface pressure and salt-induced swelling. *Langmuir*. 2000; 16:8324–8333.
34. Wu T, Gong P, Szleifer I, Vlcek P, Šubr V, Genzer J. Behavior of surface-anchored poly (acrylic acid) brushes with grafting density gradients on solid substrates: 1. Experiment. *Macromolecules*. 2007; 40:8756–8764.
35. Dong R, Lindau M, Ober C K. Dissociation behavior of weak polyelectrolyte brushes on a planar surface. *Langmuir*. 2009;25:4774–4779.
36. Aulich D, Hoy O, Luzinov I, Brücher M, Hergenröder R, Bittrich E, Eichhorn K-J, Uhlmann P, Stamm M, Esser N, Hinrichs, K. In situ studies on the switching behavior of ultrathin poly (acrylic acid) polyelectrolyte brushes in different aqueous environments. *Langmuir*. 2010;26:12926–12932.
37. Zhang L, Wang H. Photografted poly (acrylic acid) thin layers with ultra-high swelling ratios and high swelling and pH response rates. *Polymer*. 2011;52:3146–3154.
38. Boschet F, Ameduri B. (Co)polymers of chlorotrifluoroethylene: synthesis, properties, and applications. *Chem Rev*. 2014;114:927–980.
39. Yao W, Li Y, Huang X. Fluorinated poly(meth) acrylate: synthesis and properties. *Polymer*. 2014;55:6197–6211.
40. Wadekar MN, Patil YR, Ameduri B. Superior thermostability and hydrophobicity of poly(vinylidene fluoride-co-fluoroalkyl 2-trifluoromethacrylate). *Macromolecules*. 2014;47:13–25.
41. van Zoelen W, Zuckermann RN, Segalman RA. Tunable surface properties from sequence-specific polypeptoid-polystyrene block copolymer thin films. *Macromolecules* 2012;45:7072–7082.
42. Zhou Y-N, Luo Z-H, Chen J-H. Theoretical modeling coupled with experimental study on the preparation and characterization comparison of fluorinated copolymers: effect of chain structure on copolymer properties. *AIChE J*. 2013;59:3019–3033.
43. Yu H-J, Luo Z-H. Novel superhydrophobic silica/poly(siloxane-fluoroacrylate) hybrid nanoparticles prepared via two-step surface-initiated ATRP: synthesis, characterization, and wettability. *J Polym Sci A Polym Chem*. 2010;48:5570–5580.
44. Cheng DF, Masheder B, Urata C, Hozumi, A. Smooth perfluorinated surfaces with different chemical and physical natures: their unusual dynamic dewetting behavior toward polar and nonpolar liquids. *Langmuir*. 2013;29:11322–11329.
45. Cai T, Neoh KG, Kang ET, Teo SLM. Surface-functionalized and surface-functionalizable poly(vinylidene fluoride) graft copolymer membranes via click chemistry and atom transfer radical polymerization. *Langmuir*. 2011;27:2936–2945.
46. Ameduri B. Controlled radical (co)polymerization of fluoromonomers. *Macromolecules*. 2010;43:10163–10184.
47. Percec V, Guliashvili T, Ladislaw JS, Wistrand A, Stjerndahl A, Sienkowska MJ, Monteiro MJ, Sahoo, S. Ultrafast synthesis of ultrahigh molar mass polymers by metal-catalyzed living radical polymerization of acrylates, methacrylates, and vinyl chloride mediated by SET at 25 Co. *J Am Chem Soc*. 2006;128:14156–14165.
48. Matyjaszewski K, Tsarevsky NV. Macromolecular engineering by atom transfer radical polymerization. *J Am Chem Soc*. 2014;136: 6513–6533.
49. Zhang N, Samanta SR, Rosen BM, Percec V. Single electron transfer in radical ion and radical-mediated organic, materials and polymer synthesis. *Chem Rev*. 2014;114:5848–5958.
50. Anastasaki A, Nikolaou V, Nurumbetov G, Wilson P, Kempe K, Quinn JF, Davis TP, Whittaker MR, Haddleton DM. Cu (0)-mediated living radical polymerization: a versatile tool for materials synthesis. *Chem Rev*. In press.
51. Zhou Y-N, Luo Z-H. Copper (0)-mediated reversible-deactivation radical polymerization: kinetics insight and experimental study. *Macromolecules*. 2014;47:6218–6229.
52. Zhong M, Wang Y, Krys P, Konkolewicz D, Matyjaszewski K. Reversible-deactivation radical polymerization in the presence of metallic copper. Kinetic simulation. *Macromolecules*. 2013;46:3816–3827.
53. Varshney SK, Jacobs C, Hautekeer JP, Bayard P, Jerome R, Fayt R, Teyssie P. Anionic polymerization of acrylic monomers. 6. Synthesis, characterization, and modification of poly(methyl methacrylate)-poly(tert-butyl acrylate) di- and triblock copolymers. *Macromolecules*. 1991;24:4997–5000.
54. Venkataraman S, Wooley KL. ATRP from an amino acid-based initiator: A facile approach for α-functionalized polymers. *Macromolecules*. 2006;39:9661–9664.
55. Evans CM, Sandoval RW, Torkelson JM. Glass transition temperature of a component near infinite dilution in binary polymer blends: determination via fluorescence spectroscopy. *Macromolecules*. 2011; 44:6645–6648.
56. Maurer JJ, Eustace DJ, Ratcliffe CT. Thermal characterization of poly(acrylic acid). *Macromolecules*. 1987;20:196–202.
57. Park JK, Kim DW, Kim CH, Maeng KS, Hwang TS, Kim YC. Effect of drying conditions on the glass transition of poly (acrylic acid). *Polym Eng Sci*. 1991;31:867–872.
58. Wong CLH, Kim J, Torkelson JM. Breadth of glass transition temperature in styrene/acrylic acid block, random, and gradient copolymers: Unusual sequence distribution effects. *J Polym Sci B Polym Phys*. 2007;45:2842–2849.

59. Young T. An essay on the cohesion of fluids. *Philos Trans R Soc Lond* 1805;95:65–87.
60. Feng X J, Jiang L. Design and creation of superwetting/antiwetting surfaces. *Adv Mater*. 2006;18:3063–3078.
61. Tadmor R. Line energy and the relation between advancing, receding, and young contact angles. *Langmuir*. 2004;20:7659–7664.
62. Tian Y, Su B, Jiang L. Interfacial material system exhibiting superwettability. *Adv Mater*. 2014;26:6872–6897.
63. Guo Y, Tang D, Gong Z. Superhydrophobic films fabricated by electrospraying poly(methyl methacrylate)-b-poly(dodecafluoroheptyl methacrylate) diblock copolymers. *J Phys Chem C*. 2012;116: 26284–26294.
64. Zhao Z, Ni H, Han Z, Jiang T, Xu Y, Lu X, Ye P. Effect of surface compositional heterogeneities and microphase segregation of fluorinated amphiphilic copolymers on antifouling performance. *ACS Appl Mater Interfaces*. 2013;5:7808–7818.
65. Xue Z, Cao Y, Liu N, Feng L, Jiang L. Special wettable materials for oil/water separation. *J Mater Chem A*. 2014;2:2445–2460.
66. Xue Z, Wang S, Lin L, Chen L, Liu M, Feng L, Jiang L. A novel superhydrophilic and underwater superoleophobic hydrogel-coated mesh for oil/water separation. *Adv Mater*. 2011; 23: 4270-4273.
67. Yang J, Zhang Z, Xu X, Zhu X, Men X, Zhou X. Superhydrophilic-superoleophobic coatings. *J Mater Chem*. 2012;22:2834–2837.
68. Zhang L, Zhong Y, Cha D, Wang P. A self-cleaning underwater superoleophobic mesh for oil-water separation. *Sci Pep*. 2013;3: 2326.
69. Yoon H, Na S-H, Choi J-Y, Latthe SS, Swihart MT, Al-Deyab SS, Yoon SS. Gravity-driven hybrid membrane for oleophobic-superhydrophilic oil-water separation and water purification by graphene. *Langmuir*. 2014;30:11761–11769.
70. Brown PS, Atkinson O, Badyal JPS. Ultrafast oleophobic-hydrophilic switching surfaces for antifogging, self-cleaning, and oil-water separation. *ACS Appl Mater Interfaces*. 2014;6:7504–7511.
71. Zhang F, Zhang WB, Shi Z, Wang D, Jin J, Jiang L. Nanowire-haired inorganic membranes with superhydrophilicity and underwater ultralow adhesive superoleophobicity for high-efficiency oil/water separation. *Adv Mater*. 2013;25:4192–4198.
72. Dong Y, Li J, Shi L, Wang X, Guo Z, Liu W. Underwater superoleophobic graphene oxide coated meshes for the separation of oil and water. *Chem Commun*. 2014;50:5586–5589.
73. Cassie ABD, Baxter S. Wettability of porous surfaces. *Trans Faraday Soc*. 1944;40:546–551.
74. Wenzel RN. Resistance of solid surfaces to wetting by water. *Ind Eng Chem*. 1936;28:988–994.
75. Chen PC, Xu ZK. Mineral-coated polymer membranes with superhydrophilicity and underwater superoleophobicity for effective oil/water separation. *Sci Rep*. 2013;3:2776.
76. Gao X, Xu L-P, Xue Z, Feng L, Peng J, Wen Y, Wang S, Zhang X. Dual-scaled porous nitrocellulose membranes with underwater superoleophobicity for highly efficient oil/water separation. *Adv Mater*. 2014;26:1771–1775.
77. Li JJ, Zhou YN, Luo ZH. Smart fiber membrane for pH-induced oil/water separation. *ACS Appl Mater Interfaces*. 2015;7:19643–19650.
78. Zheng X, Guo Z, Tian D, Zhang X, Li W, Jiang L. Underwater self-cleaning scaly fabric membrane for oily water separation. *ACS Appl Mater Interfaces*. 2015;7:4336–4343.
79. Xu Z, Zhao Y, Wang H, Wang X, Lin T. A Superamphiphobic coating with an ammonia-triggered transition to superhydrophilic and superoleophobic for oil-water separation. *Angew Chem Int Ed*. 2015; 54:4527–4530.
80. Dunderdale GJ, Urata C, Sato T, England MW, Hozumi A. Continuous, high-speed and efficient oil/water separation using meshes with antagonistic wetting properties. *ACS Appl Mater Interfaces*. 2015;7: 18915–18919.

Manuscript received Sep. 26, 2015, and revision received Nov. 16, 2015.